Statistical uncertainties of a chiral interaction at next-to-next-to leading order

2015 J. Phys. G: Nucl. Part. Phys. 42 034003

(http://iopscience.iop.org/0954-3899/42/3/034003)

IOP Publishing Journal of Physics G: Nuclear and Particle Physics
J. Phys. G: Nucl. Part. Phys. **42** (2015) 034003 (16pp) doi:10.1088/0954-3899/42/3/034003

Statistical uncertainties of a chiral interaction at next-to-next-to leading order

A Ekström[1,8], B D Carlsson[1,2], K A Wendt[3,4], C Forssén[2], M Hjorth Jensen[1,5], R Machleidt[6] and S M Wild[7]

[1] Department of Physics and Center of Mathematics for Applications, University of Oslo, N-0316 Oslo, Norway
[2] Department of Fundamental Physics, Chalmers University of Technology, SE-412 96 Göteborg, Sweden
[3] Department of Physics and Astronomy, University of Tennessee, Knoxville, TN 37996, USA
[4] Physics Division, Oak Ridge National Laboratory, Oak Ridge, TN 37831, USA
[5] National Superconducting Cyclotron Laboratory and Department of Physics and Astronomy, Michigan State University, East Lansing, MI 4882, USA
[6] Department of Physics, University of Idaho, Moscow, ID 83844, USA
[7] Mathematics and Computer Science Division, Argonne National Laboratory, Argonne, IL 60439, USA

E-mail: ekstrom@utk.edu

Received 26 June 2014, revised 14 August 2014
Accepted for publication 15 August 2014
Published 5 February 2015

Abstract
We have quantified the statistical uncertainties of the low-energy coupling-constants (LECs) of an optimized nucleon–nucleon interaction from chiral effective field theory at next-to-next-to-leading order. In addition, we have propagated the impact of the uncertainties of the LECs to two-nucleon scattering phase shifts, effective range parameters, and deuteron observables.

Keywords: numerical optimization, nucleon–nucleon interactions, uncertainty quantification, error propagation

(Some figures may appear in colour only in the online journal)

1. Introduction

Chiral effective field theory (χ EFT [1, 2]) defines the current paradigm in the theoretical description of the interaction between the nucleons. The algebraic structure and pattern are

[8] Present address: Department of Physics and Astronomy, University of Tennessee, Knoxville, TN 37996, USA

governed by an effective Lagrangian with an associated power counting scheme. However, as in the case of any nuclear interaction, the numerical values of a set of low-energy coupling-constants (LECs) will govern the quantitative behavior of the interaction to a large extent. Thus, for a precise and successful modeling of the atomic nucleus, the numerical values of the LECs must be well-constrained. In the nucleon–nucleon (NN) sector, this is usually achieved by confronting the LECs with data from scattering experiments. The pool of fit observables consists of several thousands of measured proton–proton (pp) and neutron–proton (np) scattering cross-sections below the pion-production threshold at 290 MeV, and sometimes also the measured deuteron properties. This constitutes an extensive nonlinear optimization problem that is best tackled using mathematical optimization algorithms [3]. The experimental scattering data that constrain the microscopic interactions have well-defined statistical uncertainties. These uncertainties must propagate to the LECs of the nuclear interaction, and therefore also to any subsequently computed many-body observables.

In many cases the numerical solution of the many-body Schrödinger equation is no longer the bottleneck in nuclear modeling; see, e.g., [4]. Instead, it is the quality of the underlying nuclear Hamiltonian that is responsible for observed discrepancies between data and theory. In relation to this, it is important to note that theoretical results from nuclear models are seldomly reported with proper uncertainty estimates. However, the theoretical uncertainties and error estimates of models are increasingly acknowledged as vital for making further theoretical developments; see, e.g., [5].

In this paper we address the statistical uncertainties of the LECs of a two-nucleon interaction from χ EFT. This provides a first step toward a reliable extraction of the statistical and systematic uncertainties of nuclear many-body observables computed with *ab initio* models. We present a mathematically optimized two-nucleon interaction at next-to-next-to-leading order (NNLO). From a statistical perspective, we can view the optimization problem as a nonlinear regression problem, and therefore easily extend the analysis to investigate the statistical constraints on the LECs of this optimized interaction.

2. Nuclear forces from chiral EFT

From a historical perspective, it is interesting to see how nuclear physicists have returned to Yukawa's idea [6], at least conceptually, but this time included the important notion of a spontaneously broken chiral symmetry in the u–d quark sector of quantum chromodynamics (QCD). As a consequence, pions are emerging as pseudo-Goldstone bosons, whose interactions vanish in the low-momentum limit. A chiral nuclear force is therefore grounded in the symmetries of QCD and uses only nucleons and pions as degrees of freedom. It is well known that QCD is nonperturbative at the energy scales relevant for nuclear structure. A perturbative expansion of the nuclear force is instead constructed from an effective field theory, using the notion of a separation of scales [1, 2]. This approach boils down to taking the most general nuclear-force Lagrangian, obeying the symmetries of QCD, and subsequently expanding it in terms of (Q/Λ_x) where Q is a soft momentum-scale, typically the pion mass or momentum, and Λ_x sets the hard momentum-scale, typically on the order of the rho-meson mass. It is equipped with a power-counting scheme that governs the structure of the order-by-order expansion. At each chiral order ν, a certain number of new LECs appear. These are related to either the long-ranged and Yukawa-like pion–nucleon $(\pi - N)$ interaction or to the short-ranged, and unresolved, contact interaction. In relation to this, a long-standing problem in nuclear physics has been to systematically construct two- and higher-order nucleon

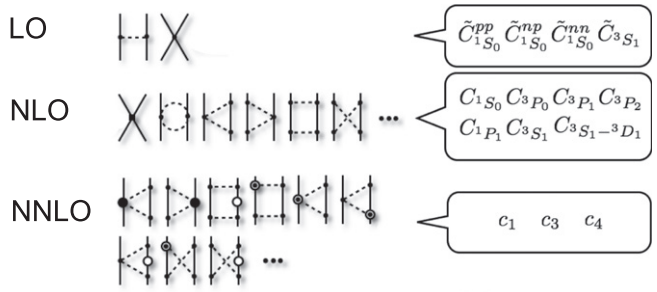

Figure 1. The hierarchy of the nuclear force in χ EFT, and in particular the two-nucleon sector up to NNLO. Solid lines indicate nucleons and dashed lines pions. The boxes on the right indicate the number and notation of the new LECs introduced at each chiral order. The $\tilde{C}$ and C parameters belong to the two-nucleon contact-potential at LO and NLO, respectively. The c_i describe the long-ranged pion-mediated physics. Note that the isospin-breaking property of the leading-order $^1S_0$ coupling-constant is a sub-leading effect. In relation to this, there exists no neutron–neutron scattering data. Thus the uncertainty of the $\tilde{C}^{nn}_{^1S_0}$ contact term will remain undetermined in this work. See the text for further details.

interactions within a common framework. This is remedied in χ EFT, where two- and higher-order interactions are borne out of the same perturbative expansion.

It was shown in [7] that it is necessary to include terms in the chiral expansion up to next-to-next-to-next-to-leading order (N3LO) (i.e., $\nu = 4$), in order for the interaction to quantitatively reproduce the combined np and pp scattering data with laboratory scattering energies up to $T_{\rm LAB} = 290$ MeV. This so-called Idaho-N3LO potential is widely used in various calculations of low-energy nuclear properties such as binding energies, radii, and excited spectra. The number of LECs grows with increasing chiral order, and at N3LO there are 34 LECs in total. Since these LECs need to be determined from experimental data, this poses a rather difficult optimization problem. It was shown in [3], that mathematical optimization algorithms can be applied successfully in order to aid in the construction of chiral potentials.

For the present investigation, we will remain at the NNLO level and treat only the two-body interaction. At this order, the dimensionality of the optimization problem is tractable while the potential is still capable of a reasonable description of low-energy nuclear physics [3]. The details of the NNLO chiral two-nucleon force that we study here are given in [2]. In brief, we use the Weinberg power counting and regulate the potential with a cutoff $\Lambda = 500$ MeV in the solution of the Lippmann–Schwinger equation. The two-pion exchange-potential is renormalized using the spectral function renormalization prescription with a cutoff $\Lambda_{\rm SFR} = 700$ MeV [8]. The familiar Yukawa-type one-pion exchange-force enters at leading-order (LO) together with a simple contact potential that will parameterize the ^{1}S$_0$ and ^{3}S$_1$ partial-waves of the interaction. The sub-leading two-nucleon interaction NLO introduces a more sophisticated contact potential that breaks the isospin of the LO contacts and parameterizes also the deuteron channel and the P- waves. At NLO the leading two-pion exchange also appears. The NNLO contribution only impacts the $\pi - N$ sector in terms of certain relativistic corrections and additional two-pion exchanges that are proportional to the LECs c_1, c_3, and c_4. In total, there are 14 LECs in the two-nucleon sector up to and including NNLO. In summary, the various orders of the irreducible graphs that define the NNLO potential are given by (figure 1)

$$V_{\mathrm{LO}} = V_{\mathrm{ct}}^{(0)} + V_{1\pi}^{(0)}, \tag{1}$$

$$V_{\mathrm{NLO}} = V_{\mathrm{LO}} + V_{\mathrm{ct}}^{(2)} + V_{1\pi}^{(2)} + V_{2\pi}^{(2)}, \tag{2}$$

$$V_{\mathrm{NNLO}} = V_{\mathrm{NLO}} + V_{1\pi}^{(3)} + V_{2\pi}^{(3)}, \tag{3}$$

where the superscript denotes the order ν of the low-momentum expansion. Contact potentials carry the subscript 'ct' and pion-exchange potentials can be identified by an obvious subscript.

3. Definition of the objective function

The optimization problem consists of determining an optimal set of values for the 13 LECs $\mathbf{x} = (\tilde{C}_{^1S_0}^{\mathrm{np}}, \tilde{C}_{^1S_0}^{\mathrm{pp}}, \ldots, c_1, c_3, c_4)$ of the NNLO interaction such that the np- and the pp-scattering data are best reproduced. Note that we will not optimize the charge-dependent neutron–neutron LO contact $\tilde{C}_{^1S_0}^{nn}$ with the other LECs, since there exists no *nn* scattering data. Instead, this contact is determined from the model-dependent extractions of the *nn* effective range parameters. We do not include any other data types in the optimization protocol either, such as the deuteron binding energy, since we have a subsequent statistical analysis of the optimum in mind. A mixture of data types would introduce an additional parameter to determine the relative importance of, for example, cross-sections versus a binding energy. Note also that we keep the axial-vector coupling constant $g_{\mathrm{A}} = 1.29$ to account for the Goldberger–Treiman discrepancy, the weak-pion decay $f_\pi = 92.4$ MeV, and all pion- and nucleon-masses fixed. It was shown in [3] that a chiral potential at NNLO with $\Lambda = 500$ MeV and $\Lambda_{\mathrm{SFR}} = 700$ MeV can describe the two-nucleon scattering data up to a laboratory scattering-energy $T_{\mathrm{LAB}} \leqslant 125$ MeV. This is therefore our cutoff in the experimental datapool used in the fit. We also note that the optimized NNLO potential presented here differs from $\mathrm{NNLO}_{\mathrm{opt}}$ [3] in terms of the definition of the objective function. The latter potential was optimized with respect to a selected class of phase shifts and the deuteron binding energy. In this study we wish to estimate the uncertainties of the LECs, and for that reason we have constructed an objective function that consists of the experimentally measured cross-sections and their associated experimental uncertainties.

The experimental data is composed of N_g groups of measurements, where each group consists of N_d measured cross-sections $\mathcal{O}_{g,d}^e \pm \sigma_{g,d}$ with a common normalization constant ν_{g} and associated error $\sigma_{g,0}$. A group of data originates from the same experiment. The normalization constant, together with its uncertainty, represents the systematic uncertainty of the measurement. For an absolute measurement, the normalization is given by $\nu_g = 1 \pm 0$. Usually, this means that the statistical and systematic errors have been combined with $\sigma_{g,d}$, but certain experiments are not normalized at all. Instead, only the angular- or T_{LAB}-dependence of the cross-section was determined. For these groups of data, so-called 'floated data', ν_{g} is solved for in the optimization by minimizing the discrepancy between the model prediction $\mathcal{O}_{g,\,d}^t$ and the experimental data points $\mathcal{O}_{g,\,d}^e$. For practical purposes the normalization error can be considered infinite in these cases, and will therefore not contribute to χ^2. Statistically, we seek to find the minimum of χ^2 with respect to variations of the (LEC) parameter vector $\mathbf{x}$. Thus, we are after a minimizer of an objective function of the form

Table 1. The experimental database consists of the SM99 database with the exclusion of the following data points.

E_{LAB}	θ_{CM}	Type	Reference
7.6	90.6	np P	[11]
16.9	all	15 np P	[12]
16.9	all	4 np P	[13]
17.0	all	6 np P	[14]
22.0	141.0	np P	[14]
29.9	164.9	np σ	[15]
54.0	—	np σ_{tot}	[16]
67.5	46.0	np σ	[17]
97.7	46.0,71.4	2 pp P	[18]

$$\chi^2(\mathbf{x}_\mu) = \min_{\mathbf{x}} \left\{ \sum_{g=1}^{N_g} \min_{\nu_g} \left[\sum_{d=1}^{N_d} \left(\frac{\nu_g \mathcal{O}^t_{g,d}(\mathbf{x}) - \mathcal{O}^e_{g,d}}{\sigma_{g,d}} \right)^2 \right] + \left(\frac{1-\nu_g}{\sigma_{g,0}} \right)^2 \right\}. \quad (4)$$

The present dataset consists of $N_{\mathrm{obs}} = 1848$ measured data points and $N_\nu = 108$ normalization constants, out of which $N_{\mathrm{float}} = 11$ data sets are floated. Thus, there are $N_{\mathrm{datum}} = N_{\mathrm{obs}} + N_\nu - N_{\mathrm{float}} = 1945$ terms in the objective function, and $N_\nu - N_{\mathrm{float}} = 97$ of them come from the normalization of certain data groups. The total number of parameters used in the optimization is $N_{\mathrm{par}} = N_{\mathrm{float}} + N_{\mathrm{NNLO}} = 24$, where $N_{\mathrm{NNLO}} = 13$ is the total number of varied parameters in the NNLO potential. The number of degrees of freedom in the optimization amounts to $N_{\mathrm{df}} = N_{\mathrm{datum}} - N_{\mathrm{par}} = 1921$. In the nuclear-interaction community, the quality of the potential is gauged by the $\chi^2/N_{\mathrm{datum}}$. However, for the statistical distributions that are applied in the statistical analysis of the potential we will use N_{df}. The present data set is based on the SM99 data set [9], with the exclusion of 7 + 25 datapoints, see table 1. Seven data points were removed based on the 3σ-rejection rule [10] with respect to a CD-Bonn prediction [9]. The origin of the discrepancy with respect to the 3σ-rejection is most likely due to slightly different numerics in the computer codes that solves the two-nucleon scattering problem. An additional 25 datapoints were removed due to numerical issues when differentiating the Lippmann–Schwinger equation of the $^3S_1 - {}^3D_1$ coupled-channel in the bound-state cross-over region around 17 MeV. The removal of these latter 25 datapoints had no significant impact on the solution of the optimization problem.

4. The optimized NNLO potential

We solve the optimization problem defined in equation (4) using an optimization-routine called POUNDerS [19, 20], which has also been applied to optimize nuclear energy density functionals [21]. The POUNDerS algorithm does not rely on derivatives of the objective function with respect to the model parameters. Instead, it solves a sequence of easier subproblems based on locally fitting a collection of quadratic surfaces to the residual values in the objective function. The vector $\mathbf{x}_\mu$ of the LECs that minimize the χ^2 in (4) is given in table 2. The value of the objective function at the minimum is $\chi^2(\mathbf{x}_\mu) = 2243.5$, which gives $\chi^2/N_{\mathrm{datum}} = 1.15$ over the T_{LAB}-range 0–125 MeV. In detail, the $\chi^2_{\mathrm{np}}/N_{\mathrm{datum}}$ in the bins $T_{\mathrm{LAB}} = 0 - 35$ MeV and $T_{\mathrm{LAB}} = 35 - 125$ MeV are 0.87 and 1.24, respectively. Similarly,

Table 2. Numerical values of the LECs for the optimized chiral NNLO potential. The optimum is defined by the $\mathbf{x}_\mu$ vector. The standard-deviation σ for each parameter, except $\tilde{C}^{nn}_{^1S_0}$, is given in the second column. A 95% confidence interval is given in the third column. See text for details.

LEC	x_μ	1σ	$1\sigma/x_\mu$ (%)	95% CI
c_1	−0.919353	5.41×10^{-2}	5.88	[−1.008365, −0.830340]
c_3	−3.889839	1.68×10^{-2}	0.43	[−3.917492, −3.862185]
c_4	4.307371	4.22×10^{-2}	0.98	[4.237956, 4.376786]
$\tilde{C}^{np}_{^1S_0}$	−0.152151	4.01×10^{-4}	0.26	[−0.152811, −0.151491]
$\tilde{C}^{pp}_{^1S_0}$	−0.151363	3.86×10^{-4}	0.25	[−0.151998, −0.150728]
$\tilde{C}^{nn}_{^1S_0}$	−0.151804	—	—	—
$\tilde{C}_{^3S_1}$	−0.158482	2.49×10^{-4}	0.16	[−0.158891, −0.158073]
$C_{^1S_0}$	2.404311	3.36×10^{-3}	0.14	[2.398774, 2.409849]
$C_{^3P_0}$	1.235001	9.51×10^{-3}	0.77	[1.219344, 1.250658]
$C_{^1P_1}$	0.414829	1.09×10^{-2}	2.62	[0.396950, 0.432707]
$C_{^3P_1}$	−0.770879	7.17×10^{-3}	0.93	[−0.782678, −0.759079]
$C_{^3S_1}$	0.927936	3.12×10^{-3}	0.34	[0.922809, 0.933064]
C_{E_1}	0.618754	2.53×10^{-3}	0.41	[0.614584, 0.622925]
$C_{^3P_2}$	−0.673469	4.54×10^{-3}	0.67	[−0.680941, −0.665996]

the $\chi^2_{\rm pp}/N_{\rm datum}$ in these bins are 1.04 and 1.53, respectively. Thus, the optimized NNLO potential quantitatively describes the np + pp scattering data below $T_{\rm LAB} = 125$ MeV and is accurate enough to model the bound-state properties of light- and medium-mass nuclei.

5. Statistical analysis

We now turn our attention to the estimation of the statistical uncertainties of the optimal LEC values $\mathbf{x}_\mu$. Formally, the analysis in this section requires that the true errors in the objective function are normally distributed and independent. Although this is a rather strong requirement and hard to fulfill rigorously, figure 2 illustrates that the residual errors for our $\mathbf{x}_\mu$ are approximately normal. Consequently, we conduct the corresponding statistical analysis in order to gain more insights into the NNLO potential. The statistical uncertainty in $\mathbf{x}_\mu$ will propagate to an uncertainty in the response of any many-body model based on this NNLO potential. As a first step, we have carried out a preliminary study on the extraction of statistical uncertainties on the LECs and propagated the errors to a selected set of deuteron observables, and quantified the uncertainties in the scattering phase-shifts as well as the effective range parameters for the $^1S_0$ channel.

5.1. Theoretical model uncertainties

In a statistical setting, the optimization of the objective function also represents a nonlinear regression problem. We can view the input vector $\mathbf{x}_\mu$ as a normally distributed random vector whose variance we seek. In order to determine the covariances of the model parameters, we follow [5] and perform a Taylor expansion of the objective function χ^2 around the mean

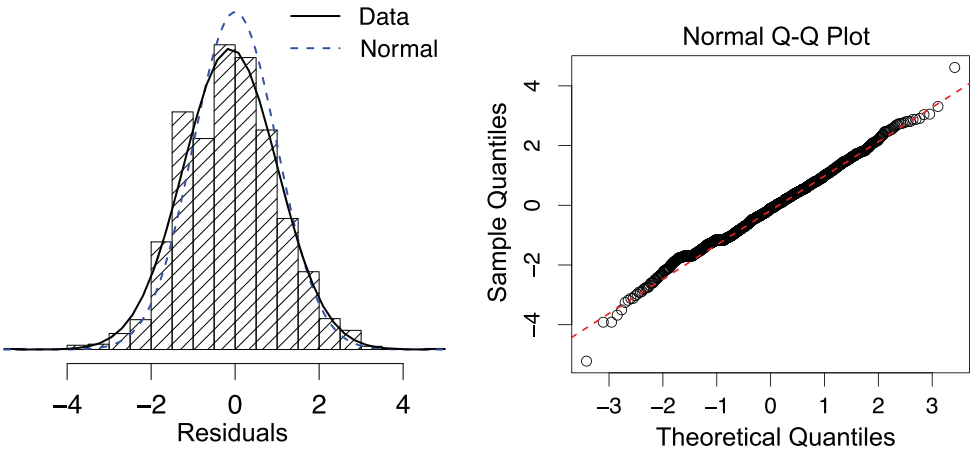

Figure 2. (Left) The residuals of the objective function at $\mathbf{x}_\mu$ are fairly normally distributed. For comparison, a standard normal ($N(0, 1)$) distribution function (blue dashed line) is also plotted. The skewness and excess kurtosis of the histogram of residuals are 0.06 and 0.37, respectively. A fitted normal distribution is indicated with a black solid line. (Right) A quantile–quantile plot that compares the normality of the residuals with the normal distribution.

vector $\mathbf{x}_\mu$:

$$\chi^2(\mathbf{x}) - \chi^2(\mathbf{x}_\mu) \approx \frac{1}{2}\sum_{i,j=1}^{N_p} \frac{\partial^2\chi^2}{\partial x_i \partial x_j}\bigg|_{\mathbf{x}=\mathbf{x}_\mu} (x_i - x_{\mu,i})(x_j - x_{\mu,j}). \tag{5}$$

The linear term drops out since $\mathbf{x}_\mu$ is a minimum. The approximations that we make in this analysis depend on staying sufficiently close to this point in parameter space. The scaled Hessian $\mathbf{H}$, with elements $H_{ij} = \frac{1}{2}\left.\frac{\partial^2\chi^2}{\partial x_i \partial x_j}\right|_{\mathbf{x}=\mathbf{x}_\mu}$, is related to the covariance matrix of the model parameters as

$$\Sigma = \frac{\chi^2}{N_{\rm df}}\mathbf{H}^{-1}. \tag{6}$$

In this analysis, we obtained the Hessian matrix $\mathbf{H}$ from a bivariate spline in the vicinity of the optimum. The square root of the diagonal elements of the covariance matrix $\Sigma = \mathrm{Cov}(\mathbf{x}_i, \mathbf{x}_j)$ are interpreted as the errors of the LECs: $\sigma_i = \sqrt{\Sigma_{ii}}$. In addition to extracting the errors, we deduce a 95% confidence interval (CI) for every parameter according to the t-distribution

$$x_{\mu,i} - \sigma_i \cdot t_{N_{\rm df},\alpha/2} \leqslant x_i \leqslant x_{\mu,i} + \sigma_i \cdot t_{N_{\rm df},\alpha/2}, \tag{7}$$

where $\alpha = 0.05$. The CI can be interpreted as the range of acceptable values for constructing the current NNLO potential. In table 2 we list statistical uncertainties of the LECs together with 95% CIs. In summary, the uncertainties are at the 1%-level, but two LECs, c_1 and C_1^{1P}, stand out and have relatively large errors. It is interesting that c_1 exhibits an approximately five times larger uncertainty compared to the other $\pi - N$ LECs. This is in qualitative agreement with the similar analysis of [22], albeit using a different representation of the short-ranged interaction. The different representation of the contact potential, or simply the fact that we are at a completely different optimum, could be the reasons for the drastically smaller

uncertainties that we observe here. In general, the *S*-wave contacts are slightly more precise compared to the *P*-wave contacts. This is perhaps not so surprising, since the *P*-wave phase-shifts are difficult to reproduce at NNLO [3]. The isoscalar $^1P_1$-contact is determined only by the np-data, which is overall much less precise compared to the pp-data.

The correlations between the LECs provide further insights into the behavior of the current model. Equipped with the covariance matrix Σ of the LECs, it is a simple task to extract the correlation coefficient between the optimal parameters $x_{\mu,i}$ and $x_{\mu,j}$ as

$$R_{ij} = \frac{\Sigma_{ij}}{\sqrt{\Sigma_{ii}\Sigma_{jj}}}. \tag{8}$$

The correlation matrix $\mathbf{R}$ is given in table 3, and a graphical representation of $\mathbf{R}$ is shown in figure 3. For this NNLO interaction, the strongest correlations occur between c_1 and the charge-dependent $^1S_0$ contacts. There is also some correlation between the three different c_i's, see figure 4. Besides these, the correlation matrix does not signal a strongly correlated set of parameters. In fact, 93% of the elements indicate a correlation $|R| < 0.80$. Both c_1/c_3 anti-correlate/correlate rather strongly with c_4, at least compared to the correlation $R(c_1, c_3)$. It should be noted that both c_1 and c_3 belong to the central part of the potential, whereas c_4 belongs to the spin–spin and tensor parts of the interaction. Thus, the observed correlations could be a weak manifestation of the expected interplay between the central and the tensor parts of the nuclear interaction [23]. Also, the anti-correlation between c_1 and c_3 of the chiral two-pion exchange potential was observed already in [22]. However, the (weaker) correlations $R(c_1, c_4)$ and $R(c_3, c_4)$ have opposite signs in the analysis of [22]. As mentioned, the LECs of the contact potential of a chiral NNLO interaction enter only in *S*- and *P*-waves. From the analysis it is clear that these two groups of LECs mostly anti-correlate. Overall, this picture of a certain partial-wave grouping is consistent with the observations made in a similar analysis based on various coarse-grained δ-shell interactions [22, 24, 25].

6. Error propagation and uncertainties of the deuteron observables

Equipped with statistical uncertainties of the LECs for the current NNLO, we proceed with an error propagation of these to the deuteron observables, $^1S_0$ effective range parameters, and selected partial-wave phase-shifts.

In general, we are after the response Y of a model $\mathcal{M}$ that depends on an input random vector $\mathbf{X}$, and thus the response itself becomes a random vector. For the present application, we can restrict the model to a scalar-valued mathematical function $\mathcal{M}: \mathbb{R}^M \to \mathbb{R}$. The response Y is a random variable given by

$$Y = \mathcal{M}(\mathbf{X}), \tag{9}$$

and we seek the variance of the probability density function (pdf) $f_Y(y)$, which will depend on the pdf of the input $\mathbf{f}_\mathbf{X}(\mathbf{x})$. Here, we will use a derivative-based approximation to the response variance σ_Y. This will require the computation of as many derivatives $\frac{\partial \mathcal{M}}{\partial x_i}$ as there are parameters x_i, but will not produce a pdf $f_Y(y)$ for the response. Another alternative for propagating the uncertainties of the LECs would be to do a simple Monte Carlo sampling of a normally distributed nuclear interaction. That is, to compute the observable of interest N_{MC} times using an interaction with a normally distributed set of LECs. We carried out such an analysis, and the results are nearly identical to the computationally less expensive method based on error propagation by means of perturbation.

Table 3. Correlation matrix for the NNLO potential $\mathbf{x}_\mu$.

	c_1	c_3	c_4	$\tilde{C}^{\rm np}_{^1S_0}$	$\tilde{C}^{\rm pp}_{^1S_0}$	$\tilde{C}_{^3S_1}$	$C_{^1S_0}$	$C_{^3P_0}$	$C_{^1P_1}$	$C_{^3P_1}$	$C_{^3S_1}$	C_{E_1}	$C_{^3P_2}$
c_1	1.00												
c_3	−0.39	1.00											
c_4	−0.76	0.68	1.00										
$\tilde{C}^{\rm np}_{^1S_0}$	0.96	−0.48	−0.78	1.00									
$\tilde{C}^{\rm pp}_{^1S_0}$	0.98	−0.48	−0.79	0.99	1.00								
$\tilde{C}_{^3S_1}$	0.09	0.03	0.23	0.08	0.07	1.00							
$C_{^1S_0}$	0.49	−0.64	−0.37	0.40	0.42	0.23	1.00						
$C_{^3P_0}$	−0.71	0.48	0.74	−0.69	−0.70	0.07	−0.46	1.00					
$C_{^1P_1}$	−0.12	0.32	0.22	−0.19	−0.19	−0.14	−0.08	0.06	1.00				
$C_{^3P_1}$	−0.64	0.40	0.51	−0.64	−0.65	−0.08	−0.39	0.36	0.18	1.00			
$C_{^3S_1}$	0.60	−0.55	−0.44	0.61	0.62	−0.07	0.59	−0.45	−0.16	−0.40	1.00		
C_{E_1}	−0.07	0.29	0.46	−0.09	−0.10	−0.09	0.06	0.23	0.26	−0.01	−0.11	1.00	
$C_{^3P_2}$	−0.79	0.85	0.89	−0.84	−0.84	0.02	−0.62	0.67	0.30	0.61	−0.65	0.28	1.00

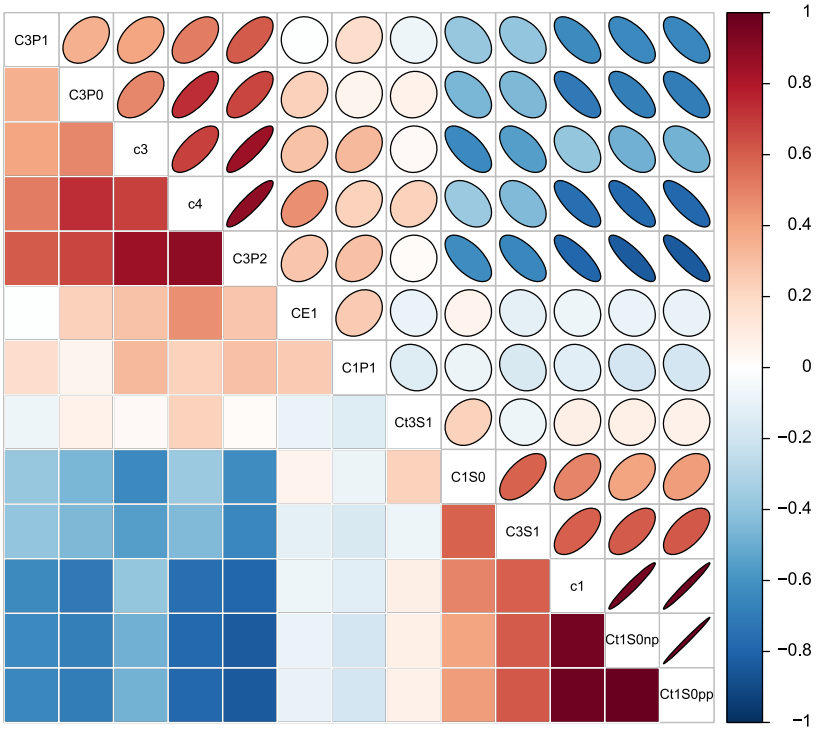

Figure 3. Graphical representation of the correlation matrix for the current NNLO potential. Maximum correlation and anti-correlation are indicated with blue and red colors, respecively. The upper triangle contains all the correlation ellipses. The matrix has been grouped in blocks of similar correlation. The block structure of the *S*- and *P*-wave correlations is clearly visible. See the text for details.

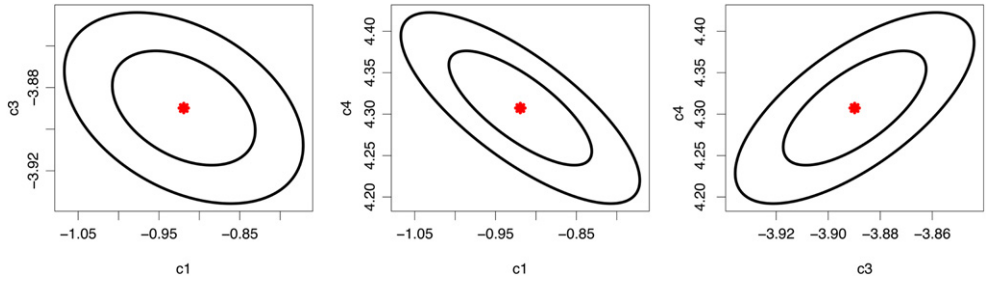

Figure 4. Correlations between the c_1, c_3, and c_4 LECs at the current NNLO optimum. The inner and outer contours trace the 95% and 99% confidence ellipses, respectively.

6.1. Error propagation by means of perturbation

A Taylor series expansion of the model $\mathcal{M}(\mathbf{x})$ around its mean value $\mathbf{x}_\mu$ is given by

$$Y = \mathcal{M}(\mathbf{x}) = \mathcal{M}(\mathbf{x}_\mu) + \sum_{i=1}^{N} \left.\frac{\partial \mathcal{M}}{\partial x_i}\right|_{\mathbf{x}=\mathbf{x}_\mu} (x_i - x_{\mu,i}) + \frac{1}{2}\sum_{i,j=1}^{N} \left.\frac{\partial^2 \mathcal{M}}{\partial x_i \partial x_j}\right|_{\mathbf{x}=\mathbf{x}_\mu} (x_i - x_{\mu,i})(x_j - x_{\mu,j}) + \cdots. \tag{10}$$

From the definition and linearity of the statistical expectation-value operator $E[\cdot]$, and assuming that $\mathbf{x}_\mu$ is a minimizer of $\mathcal{M}$ we have

$$E[Y] = E[\mathcal{M}(\mathbf{x})] \approx \mathcal{M}(\mathbf{x}_\mu) + \frac{1}{2}\sum_{i,j=1}^{N} \left.\frac{\partial^2 \mathcal{M}}{\partial x_i \partial x_j}\right|_{\mathbf{x}=\mathbf{x}_\mu} \mathrm{Cov}(x_i, x_j), \tag{11}$$

where we also identified the covariance $\mathrm{Cov}(x_i, x_j) = E[(x_i - x_{\mu,i})(x_j - x_{\mu,j})]$. The variance of the response is defined as

$$\mathrm{Var}[Y] = E[(Y - E[Y])^2]. \tag{12}$$

This can be approximated using the first-order term in the expansion of $\mathcal{M}$ in equation (10)

$$\mathrm{Var}[Y] \approx E\left[\left(\sum_{i=1}^{N} \left.\frac{\partial \mathcal{M}}{\partial x_i}\right|_{\mathbf{x}=\mathbf{x}_\mu} (x_i - x_{\mu,i})\right)^2\right] = \mathbf{J}\Sigma\mathbf{J}^T, \tag{13}$$

where $\mathbf{J}$ is the Jacobian row-vector $\mathbf{J} = [\frac{\partial \mathcal{M}}{\partial x_1}, \frac{\partial \mathcal{M}}{\partial x_2}, \ldots, \frac{\partial \mathcal{M}}{\partial x_N}]$, and Σ is the covariance matrix of the LECs. As mentioned, this is a relatively computationally inexpensive method for estimating the variance of the model prediction. It only requires the computation of $N = 13$ partial derivatives in the present case. The resulting central values as well as the propagated LEC uncertainties are given in table 4. Overall, the experimental values are more precise than their theoretical counterpart. Also, the predictions of the NNLO model are not consistent with the experimental values in all cases. In particular, the deuteron radius and quadrupole moment are both underestimated. The discrepancies are not so severe, and we note that the values that are presented here are almost identical to what is obtained using high-precision interaction models[9]. The ground state energy of the deuteron has a relative theoretical error of 0.4%. Thus, the statistical uncertainty of the interaction generates an error that is 10^4 times greater than the experimental uncertainty. Regarding the uncertainties of the effective range parameters, they again reflect the fact that the pp scattering data is more precise than the np data. Our model predictions for the pp parameters are consistent with the analysis of [26]. We have also determined the uncertainties for a selected set of partial-wave phase shifts; see table 5 and plotted in figure 5. Not surprisingly, the uncertainties increase with increasing T_{LAB}. This is most likely due to the fact that the chiral NNLO interaction is a low-momentum theory, and that the current potential is optimized only to data with $T_{\mathrm{LAB}} \leqslant 125$ MeV. Thus, values beyond this cutoff are extrapolations. Qualitatively, the results of asimilar analysis using the chiral two-pion exchange, coupled to a coarse-grained representation of the short-ranged potential, exhibits a similar pattern in the uncertainties.

[9] See for example the CD-Bonn [9] interaction model.

Table 4. Statistical uncertainties of the deuteron observables, the deuteron D-state probability P_D, and the $^1S_0$ effective range parameters that originate from the statistical uncertainty of the interaction. The energies, radii, effective range parameters, and electric moments are given in units of Mev, fm, fm, and e-fm, respectively. The P_D is reported in %. See the text for further details.

Observable	Theory	Experiment	References
	$^1S_0$ effective range		
a_{pp}^C	−7.811(1)	−7.8196(26)	[10]
		−7.8149(29)	[26]
r_{pp}^C	2.754(2)	2.790(14)	[10]
		2.769(14)	[26]
a_{np}	−23.74(17)	−23.740(20)	[9]
r_{np}	2.683(2)	2.77(5)	[9]
a_{nn}	−18.95	−18.95(40)	[27, 28]
r_{nn}	2.79	2.75(11)	[29]
	^{2}H		
E_{gs}	−2.222(8)	2.22456627(46)	[30]
$\langle r_m^2 \rangle^{1/2}$	1.968(3)	1.97535(85)	[31]
P_D	4.04(4)	—	
Q_{gs}	0.272(1)	0.2859(3)	[32, 33]

6.2. Sensitivity analysis of the model response

In order to better understand the variance of the computed observables, we quantify the relative importance of each input parameter in a linearized sensitivity analysis. In general, an approximate expression for the response variance around a nominal value $\mathbf{x}_\mu$, obtained by disregarding parameter correlations, is given by

$$\mathrm{Var}[Y] \equiv \sigma_Y^2 \approx \sum_{i=1}^{N} \left(\left. \frac{\partial \mathcal{M}}{\partial x_i} \right|_{\mathbf{x}=\mathbf{x}_\mu} \right)^2 \sigma_{x_i}^2. \tag{14}$$

This allows us to define the linearized relative importance, or sensitivity, of parameter x_i on the variance of the response Y as

$$S_i = \left(\frac{\partial \mathcal{M}}{\partial x_i} \right)^2 \left(\frac{\sigma_{x_i}}{\sigma_Y} \right)^2. \tag{15}$$

In the case of independent variables x_i, the sum of parameter sensitivities is normalized to one (i.e., $\sum_{i=1}^{N} S_i = 1$). However, for correlated input, as in our case, the sum will not add up to unity. Still, we have carried out this analysis for all deuteron observables that we have computed in this paper, see table 6. This analysis reveals the relative importance of the various sources of uncertainty when the structure of the nuclear wave function is taken into account. It is clear that the largest component of the uncertainties for the deuteron observables originate in the $\pi - N$ LECs c_1, c_3, c_4, at least for the current optimum $\mathbf{x}_\mu$.

Table 5. Selected proton–proton and neutron–proton scattering phase shifts relevant at NNLO. Note that the potential has been optimized with respect to scattering data with $T_{\mathrm{LAB}} \leqslant 125$ MeV. The remaining np and pp phase shifts have <0.001 degrees in statistical uncertainty. See the text for details.

T_{LAB}	$pp\,^1S_0$	$pp\,^3P_1$	$pp\,^3P_0$	$pp\,^3P_2$	$np\,^1S_0$	$np\,^3S_1$	$np\varepsilon_1$	$np\,^1P_1$	$np\,^3P_1$	$np\,^3P_0$	$np\,^3P_2$
1	32.80	−0.08	0.14	0.014	62.05	147.74	0.11	−0.19	−0.11	0.18	0.02
	±0.00	±0.00	±0.00	±0.00	±0.02	±0.00	±0.00	±0.00	±0.00	±0.00	±0.00
5	54.96	−0.89	1.62	0.22	63.58	118.15	0.68	−1.54	−0.92	1.66	0.25
	±0.00	±0.00	±0.00	±0.00	±0.00	±0.00	±0.00	±0.00	±0.00	±0.00	±0.00
10	55.38	−2.03	3.84	0.65	59.87	102.56	1.17	−3.16	−2.02	3.74	0.71
	±0.00	±0.00	±0.00	±0.00	±0.00	±0.00	±0.00	±0.00	±0.00	±0.00	±0.00
25	48.88	−4.84	8.82	2.50	50.67	80.45	1.82	−6.59	−4.77	8.36	2.58
	±0.00	±0.00	±0.00	±0.00	±0.00	±0.00	±0.00	±0.00	±0.00	±0.001	±0.00
50	39.09	−8.25	11.50	5.87	39.95	62.28	2.18	−10.00	−8.18	10.72	5.94
	±0.00	±0.00	±0.00	±0.00	±0.00	±0.00	±0.00	±0.00	±0.00	±0.00	±0.00
100	24.82	−14.03	7.47	10.76	25.28	41.90	2.56	−14.39	−14.06	6.50	10.75
	±0.01	±0.00	±0.01	±0.00	±0.01	±0.01	±0.01	±0.03	±0.00	±0.01	±0.00
150	14.27	−20.21	−0.78	12.64	14.71	28.40	2.81	−18.09	−20.36	−1.80	12.53
	±0.02	±0.01	±0.03	±0.00	±0.02	±0.03	±0.02	±0.13	±0.01	±0.03	±0.00
200	6.06	−27.13	−10.50	12.29	6.59	17.97	2.82	−21.60	−27.38	−11.53	12.12
	±0.05	±0.02	±0.04	±0.01	±0.05	±0.06	±0.06	±0.35	±0.03	±0.04	±0.01
250	−0.14	−34.63	−20.80	10.58	0.55	9.56	2.47	−24.78	−34.96	−21.83	10.36
	±0.10	±0.05	±0.06	±0.01	±0.11	±0.10	±0.13	±0.74	±0.05	±0.06	±0.01
300	−4.25	−42.35	−31.21	8.16	−3.39	2.93	1.65	−27.22	−42.72	−32.22	7.93
	±0.18	±0.08	±0.10	±0.02	±0.19	±0.16	±0.22	±1.36	±0.09	±0.10	±0.02
350	−6.17	−49.76	−41.23	5.56	−5.17	−1.86	0.39	−28.28	−50.13	−42.20	5.34
	±0.28	±0.14	±0.14	±0.02	±0.28	±0.23	±0.32	±2.20	±0.15	±0.15	±0.02

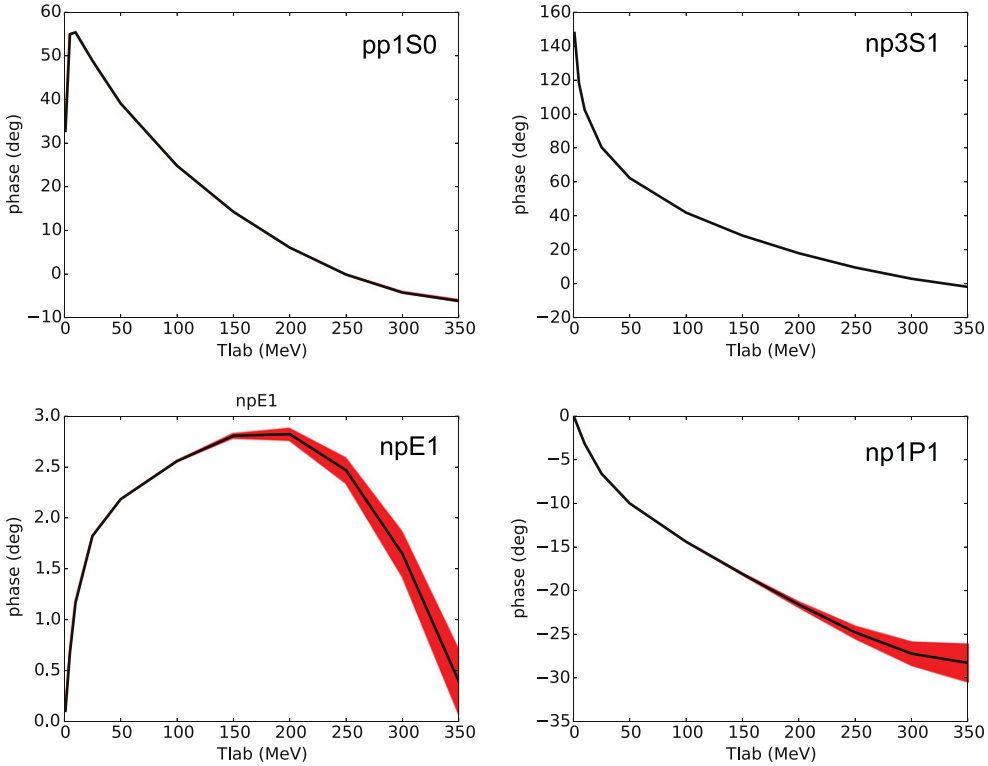

Figure 5. Selected proton–proton and neutron–proton scattering phase shifts. The statistical 1σ uncertainties from the covariance matrix of the NNLO interaction are indicated with a red band. Only for the $npE1$ and $np1P1$ phase shifts are the statistical uncertainties visible when plotted on a scale set by the magnitude of the phase shift.

Table 6. Sensitivity or importance S_i, in percent, of the different NNLO LECs with respect to the variance of the calculated deuteron properties. The values are normalized with respect to the uncorrelated uncertainties. A large number indicates that the LEC has a large impact on the uncertainty of the observable.

Obs.	c_1	c_3	c_4	$\tilde{C}_{^3S_1}$	$C_{^3S_1}$	C_{E_1}
			^{2}H			
E_{gs}	28.05	8.08	46.87	5.80	4.81	6.40
$\langle r_m^2 \rangle^{1/2}$	28.32	8.59	46.30	5.63	5.16	6.00
P_D	8.48	3.32	70.36	1.66	1.86	14.32
Q_{gs}	34.31	10.48	38.62	6.63	6.25	3.71

7. Conclusions

In conclusion, we have optimized a chiral NNLO two-body potential and quantified the statistical uncertainties of the LECs. The relative uncertainties are below 1% except for c_1 and $C_{^1P_1}$ where it is 5.84% and 2.60%, respectively. From a correlation analysis of the parameters we observed that the two groups of S-wave and P-wave contacts mostly anti-correlate. The

groupwise correlation between partial-waves of different angular momentum is consistent with similar analyses of coarse-grained nuclear potentials [22, 24, 25].

The uncertainties of the LECs are reflected in a statistical uncertainty of calculated deuteron observables, phase shifts, and effective range parameters. In general, the relative uncertainty of the theoretical results are roughly 0.5%, which is on the order of the uncertainties of the LECs. Naturally, only the lightest nuclear systems can be solved exactly using numerical methods. Before proceeding with a similar analysis for heavier systems, it can be of importance to extract the derivatives of the objective function with higher numerical precision than what can be offered from finite-difference approximations or a bivariate spline of the objective function. One way of obtaining the necessary derivatives to machine precision is automatic differentiation [34], an approach that we are actively pursuing. Also, when using certain many-body methods or employing various truncations for solving the Schrödinger equation, the propagated statistical uncertainty could become conflated with the uncertainties inherent to the numerical solution of the many-body problem. Thus, for accurate uncertainty estimates of nuclear models it is important to derive mathematically sound error estimates of the nuclear many-body method itself. This is of course relevant for an accurate extraction of the systematic uncertainty, which is always a much more complicated source of uncertainty [5].

Acknowledgments

This work was supported by the Research Council of Norway under contract ISP-Fysikk/216699; by the Office of Nuclear Physics, US Department of Energy (Oak Ridge National Laboratory), under grant nos. DE-FG02–03ER41270 (University of Idaho), DE-FG02–96ER40963 (University of Tennessee), DE-AC02–06CH11357 (Argonne), and DE-SC0008499 (NUCLEI SciDAC collaboration); and by the European Research Council under the European Community's Seventh Framework Programme (FP7/2007–2013)/ERC grant agreement no. 240603. This research used computational resources of the Notur project in Norway and the National Supercomputer Centre (NSC) at Linkoping University provided by the Swedish National Infrastructure for Computing (SNIC).

References

[1] Epelbaum E, Hammer H-W and Meißner U-G 2009 Modern theory of nuclear forces *Rev. Mod. Phys.* **81** 1773–825
[2] Machleidt R and Entem D R 2011 Chiral effective field theory and nuclear forces *Phys. Rep.* **503** 1–75
[3] Ekström A *et al* 2013 Optimized chiral nucleon–nucleon interaction at next-to-next-to-leading order *Phys. Rev. Lett.* **110** 192502
[4] Binder S, Langhammer J, Calci A and Roth R 2014 *Ab initio* path to heavy nuclei *Phys. Lett.* B **736** 119–23
[5] Dobaczewski J, Nazarewicz W and Reinhard P-G 2014 Error estimates of theoretical models: a guide *J. Phys. G: Nucl. Part. Phys.* **41** 074001
[6] Yukawa H 1935 *Proc. Phys. Math. Soc. Japan* **17** 48
[7] Entem D R and Machleidt R 2003 Accurate charge-dependent nucleon–nucleon potential at fourth order of chiral perturbation theory *Phys. Rev.* C **68** 041001
[8] Epelbaum E, Glöckle W and Meiner U-G 2004 Improving the convergence of the chiral expansion for nuclear forces II: low phases and the deuteron *Euro. Phys. J.* A **19** 401–12
[9] Machleidt R 2001 High-precision, charge-dependent Bonn nucleon–nucleon potential *Phys. Rev.* C **63** 024001
[10] Bergervoet J R, van Campen P C, van der Sanden W A and de Swart J J 1988 Phase shift analysis of 0–30 MeV pp scattering data *Phys. Rev.* C **38** 15–50

[11] Weisel G J, Tornow W, Howell C R, Felsher P D, Alohali M, Chen Z P, Walter R L, Lambert J M, Treado P A and Slaus I 1992 Neutron–proton analyzing power data between 7.6 and 18.5 MeV *Phys. Rev.* C **46** 1599–606
[12] Tornow W, Howell C R, Roberts M L, Felsher P D, Chen Z M, Walter R L, Mertens G and Šlaus I 1988 Low-energy neutron–proton analyzing power and the new Bonn potential and Paris potential predictions *Phys. Rev.* C **37** 2326–31
[13] Morris C L, O'Malley T K, May J W and Thornton S T 1974 Neutron–proton polarization measurements near 20-MeV incident neutron energy *Phys. Rev.* C **9** 924–8
[14] Wilczynski J, Hansmeyer J, Brady F P, Doll P, Heeringa W, Hiebert J C, Klages H O and Plischke P 1984 Measurements of the neutron–proton analyzing power in the energy range from 17 to 50 MeV *Nucl. Phys.* A **425** 458–68
[15] Fink G, Doll P, Ford T D, Garrett R, Heeringa W, Hofmann K, Klages H O and Krupp H 1990 Backward angle np differential cross sections from 22 to 50 MeV *Nucl. Phys.* A **518** 561–71
[16] Lisowski P W, Shamu R E, Auchampaugh G F, King N S P, Moore M S, Morgan G L and Singleton T S 1982 Search for resonance structure in the np total cross section below 800 mev *Phys. Rev. Lett.* **49** 255–9
[17] Bersbach A J, Mischke R E and Devlin T J 1976 Neutron–proton forward elastic scattering from 58 to 391 MeV *Phys. Rev.* D **13** 535–53
[18] Wigan M R, Bell R A, Martin P J, Jarvis O N and Scanlon J P 1968 Measurements of the differential cross section and polarization in proton–proton scattering at about 98 MeV *Nucl. Phys.* A **114** 377–91
[19] Wild S M 2014 Solving derivative-free nonlinear least squares with POUNDERS *Preprint* ANL/MCS-P5120-0414 (Argonne, IL: Argonne National Laboratory)
[20] Munson T, Sarich J, Wild S M, Benson S and McInnes L C 2012 TAO 2.0 users manual *Tech. Memo.* ANL/MCS-TM-322 (Argonne, IL: Argonne National Laboratory)
[21] Kortelainen M, Lesinski T, Moré J, Nazarewicz W, Sarich J, Schunck N, Stoitsov M V and Wild S 2010 Nuclear energy density optimization *Phys. Rev.* C **82** 024313
[22] Navarro Pérez R, Amaro J E and Ruiz Arriola E 2014 Coarse-grained NN potential with chiral two-pion exchange *Phys. Rev.* C **89** 024004
[23] Machleidt R 1989 The meson theory of nuclear forces and nuclear structure (*Advances in Nuclear Physics* vol 19) ed J W Negele and Erich Vogt (New York: Springer) pp 189–376
[24] Navarro Pérez R, Amaro J E and Ruiz Arriola E 2013 Partial-wave analysis of nucleon–nucleon scattering below the pion-production threshold *Phys. Rev.* C **88** 024002
[25] Navarro Pérez R, Amaro J E and Ruiz Arriola E 2013 Coarse-grained potential analysis of neutron-proton and proton–proton scattering below the pion production threshold *Phys. Rev.* C **88** 064002
[26] van der Sanden W A, Emmen A H and de Swart J J 1983 *Technical Report* THEF-NYM-83.11 Nijmegen (unpublished)
[27] Trotter D E Gonzalez *et al* 2006 Neutron-deuteron breakup experiment at $E_n = 13$ MeV: Determination of the $^1S_0$ neutron–neutron scattering length a_{nn} *Phys. Rev.* C **73** 034001
[28] Chen Q *et al* 2008 Measurement of the neutron–neutron scattering length using the π^- d capture reaction *Phys. Rev.* C **77** 054002
[29] Miller G A, Nefkens B M K and Šlaus I 1990 Charge symmetry, quarks and mesons *Phys. Rep.* **194** 1–116
[30] Mohr P J, Taylor B N and Newell D B Nov 2012 Codata recommended values of the fundamental physical constants: 2010 *Rev. Mod. Phys.* **84** 1527–605
[31] Huber A, Udem Th, Gross B, Reichert J, Kourogi M, Pachucki K, Weitz M and Hänsch T W 1998 Hydrogen-deuterium 1s-2s isotope shift and the structure of the deuteron *Phys. Rev. Lett.* **80** 468–71
[32] Bishop D M and Cheung L M 1979 Quadrupole moment of the deuteron from a precise calculation of the electric field gradient in D_2 *Phys. Rev.* A **20** 381–4
[33] Ericson T E O and Rosa-Clot M 1983 The deuteron asymptotic d-state as a probe of the nucleon–nucleon force *Nucl. Phys.* A **405** 497–533
[34] Griewank A and Walther A 2008 *Evaluating Derivatives: Principles and Techniques of Algorithmic Differentiation* (Philadelphia: SIAM)